Ibn Al-Haitham Journal for Pure and Applied Sciences
Journal homepage: jih.uobaghdad.edu.iq
PISSN: 1609-4042, EISSN: 2521-3407
IHJPAS. 2026; 39(2)

# Eco-friendly Green Synthesis of Zinc Oxide Nanoparticles from different Plant Extracts: Structural and Optical Characterization

**Raghad A. Rasheed[1], and Maysoon F.A. Alias[2]***
[1,2]Department of Physics, College of Sciences, University of Baghdad, Baghdad, Iraq
*Corresponding Author

Received:25/October/2025
Accepted:9/February/2026
Published: 20/April/2026
doi.org/10.30526/39.2.4312



**Abstract**

To create nanoparticles of zinc oxide (ZnO), a green chemistry method was used. Using *Cordia myxa* (ZnO-C) and *Ziziphus spina* (ZnO-Z) extracts works like natural reduction and stabilization properties. The green process provided enhanced phytochemical interactions, which facilitated nanoparticle formation and improved stability. The concentrations of Zn and O elements were validated using energy-dispersive X-ray spectroscopy. The ZnO-C and ZnO-Z polycrystalline structures with a hexagonal wurtzite phase were validated by X-ray diffraction (XRD), where the average crystalline size is about 17.54 nm for ZnO-C, while for ZnO-Z it is equal to 16.809 nm. Field emission scanning electron microscopy (FESEM) micrograph of ZnO-C observed to be spherical, aggregated, and ranging between 35 and 52 nm in size, whereas the FESEM micrograph of ZnO-Z showed slightly larger particles ranging from 35 to 55 nm, which were also spherical to quasi-spherical particles with a tendency to form aggregated clusters. The optical properties of ZnO nanoparticles were examined using UV-Vis spectroscopy, indicating that ZnO-C has a 3.23 eV band gap, while for ZnO-Z it is 3.37 eV. As a result, ZnO nanoparticles have been confirmed to be created using an ecofriendly method for various applications.

**Keywords:** Green synthesis, Zinc oxide Nanoparticles, Structure, Morphology and optical properties

## 1.Introduction

Research on nanomaterials has been advancing quickly and holds promise for a number of fields, such as biomedicine, optoelectronics, magnetic sciences, biosensors, and catalysis, because of their simple work-up procedure, natural environmental friendliness, affordability, and reusability[1]. Metal nanoparticles are metals with sizes between 10 and 100 nanometers. Metallic nanoparticles have special characteristics[2]. Green synthesis of nanomaterials, including zinc oxide, magnesium oxide, cerium oxide and titanium dioxide has been carried out extensively in recent years[3-5].

Environmentally friendly processes were used to create different metal oxide nanoparticles [6]. Green syntheses are the processes that have been proposed. The green synthesis technique creates nanoparticles by combining plants with salts like nitrates, chlorides, or sulfates [7]. Reducers and capping agents are contained in plant extracts. Different nanoparticles have been made from many parts of a plant that can be harvested, including the stem, leaves, roots, seeds, fruits, and flower buds [8].

Zinc oxide (ZnO) has high chemical and mechanical stability, as well as a wide range of electrical and optical properties; it has gained technological significance, allowing it to be used for engineering and medical applications such as gas sensors, flat panel displays, and antibacterial agents [9, 10]. ZnO, an n-type semiconductor of the II-VI group, consists of wurtzite crystals and has a broad, straight band; there is an energy gap of 3.37 eV. It is commonly found

in optoelectronic devices such as laser diodes, which emit blue and ultraviolet light [11-13]. Due to their unique shape (shape, size, crystalline structure, cost-effectiveness, low toxicity, and biocompatibility), ZnO nanoparticles are considered some of the most important metal oxide nanoparticles [14,15]. This research paper aims to prepare and characterize ZnO nanoparticles using *Cordia myxa* and *Ziziphus spina* extracts and investigate their structural and optical characteristics.

## 2. Materials and Methods

### 2.1. Materials

*Cordia myxa* and *Ziziphus spina* plant leaves were collected from the University of Baghdad's College of Science's garden, and zinc chloride ($ZnCl_2$), and ammonium hydroxide ($NH_4OH$) were purchased from the Alpha Chemika India Company and deionized water (DW).

### 2.2. Methods

#### 2.2.1. Biosynthesis of Plant Extracts and ZnO Nanoparticles (ZnONPs)

Multiple fresh tree leaves such as (*Cordia myxa* and *Ziziphus spina*, were brought) and washed thoroughly with triple distilled water and then were later dried. Zinc chloride ($ZnCl_2$) and ammonium hydroxide ($NH_4OH$) were purchased from the Alpha Chemika India Company, and deionized water (DW) was used. With an electric grinder, the dried leaves of the plant (*cordia myxa and ziziphus spina*) were ground, and plastic containers held their powder.

A regulated amount of distilled deionized water was mixed with the plant powder (1:10), i.e., 10 milliliters of water for every gram of plant, after 30 minutes of vigorous stirring at 70°C.

The extracts were filtered using Whatman filter paper No. 1, and the filtrate was then stored in a refrigerator at 4°C [16]. Each extract was prepared separately. In a green method, to reach a concentration of (1M), ZnO nanoparticles were produced by adding $ZnCl_2$ to 100 ml of DW using **Equation 1**[17]:

$$M_0 = \left(\frac{W_t}{M.W_t}\right) * \left(\frac{1000}{v}\right) \quad \textbf{(1)}$$

Where $M_o$ represents the concentration in molar terms (mol/L), $M.W_t$ stands for molecular weight (g/mol), $W_t$ is weight (g), and V is solution volume (mL). After that, 25 ml of plant extract is added, followed by 98% pure ($NH_4OH$) and stirring at 70-80°C for 1 hour. During centrifugation, the sediment was spun at 4,000 rpm for 15 minutes.

To achieve a pH of 7, several washes of DW were conducted[18]. After the mixture was prepared, in a 400°C crucible, it was heated for two hours [19, 20].

The thickness of the drop-cast for ZnO thin films produced by the green method was estimated using the gravimetric method (around 200 nm).

To calculate the mass difference (Δm), the glass substrates were precisely weighed both before and after the deposition procedure using an analytical balance. The film thickness (t) was calculated using **Equation 2** [21, 22]:

$$t = \Delta m / \rho A \quad \textbf{(2)}$$

Where ρ is the ZnO density and A is the effective coated area. The study's goal is to investigate ZnO nanoparticle manufacturing using aqueous extracts of *Cordia myxa* plant leaves as a stabilizing and reducing agent[23] and *Ziziphus spina* plant leaves as a capping and stabilizing agent to prevent the agglomeration of the nanoparticles [24, 25], as well as how this procedure affects the resulting nanoparticles' composition and characteristics. **Figure 1** illustrates all these processes.

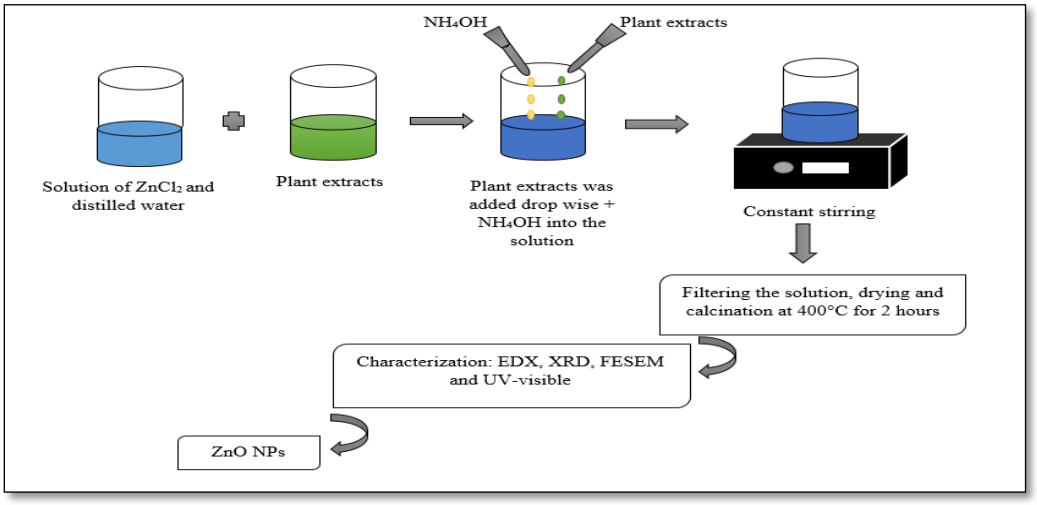


**Figure 1**. Diagram of ZnO nanoparticle synthesis.

### 2.2.2. Characterization of ZnONPs

In this study, the samples' composition was determined using energy dispersive X-ray spectroscopy (EDX), and the produced ZnO nanoparticles were characterized. ZnO nanoparticles structure and crystallite size have been characterized by X-ray diffraction. In order to find out the morphological characteristics of the produced nanoparticles, a field emission scanning electron microscopy (FESEM) was utilized, and to examine their optical properties, UV-Vis spectroscopy was used.

## 3. Results

### 3.1. Energy Dispersive X-ray Spectroscopy (EDX)

**Figures 2** and **3** showed the EDX analysis, which was used to analyze and confirm the elemental composition (quantitative elemental structure) of greenly synthesized ZnO nanoparticles using ZnO-C and ZnO-Z extracts. The EDX spectrum of ZnO NPs using *Cordia myxa and Ziziphus spina* extract made it evident distinct peaks are present; the first for zinc is the $K_\alpha$ line (8.6-8.7 keV), $K_\beta$ (9.5-9.6) keV, and $L_\alpha$ (1.0 - 1.1) keV), and the second for oxygen is at ($K_\alpha$ =0.525 keV). With changes based on the plant extract utilized in the synthesis, these data demonstrate that Zn and O are the main elements in both samples.

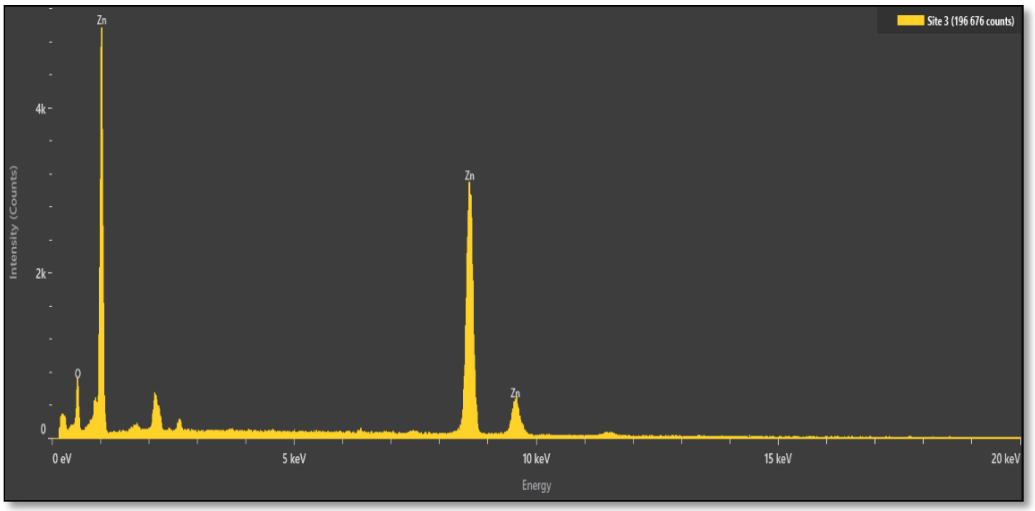


**Figure 2.** EDX for ZnO-C-NPs

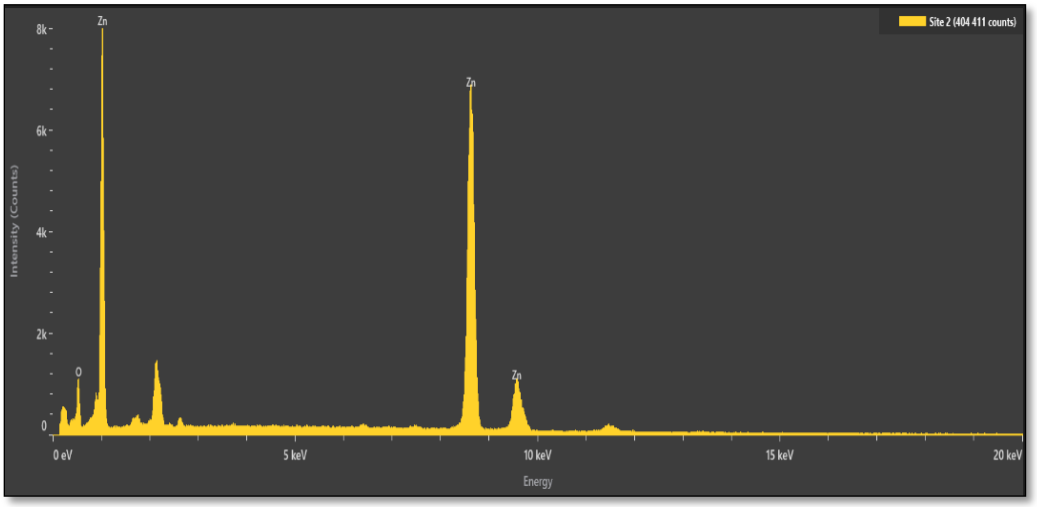


**Figure 3**. EDX for ZnO-Z-NPs

## 3.2. X-Ray Diffraction (XRD)

X-ray diffraction (XRD) patterns of ZnO NPs nanoparticles were used to determine the nanoparticle structure, Miller modulus, phase, and crystallite size. A zinc oxide X-ray diffraction (XRD) pattern was shown in **Figure 4a** for *Cordia myxa* extract ZnO- C powder, while **Figure 4b** illustrated the zinc oxide X-ray diffraction (XRD) patterns that were prepared using *Ziziphus spina* extract ZnO-Z. **Tables 1** and **2** showed the X-ray parameters for ZnO-C and ZnO-Z respectively. These results are in agreement with other researchers.

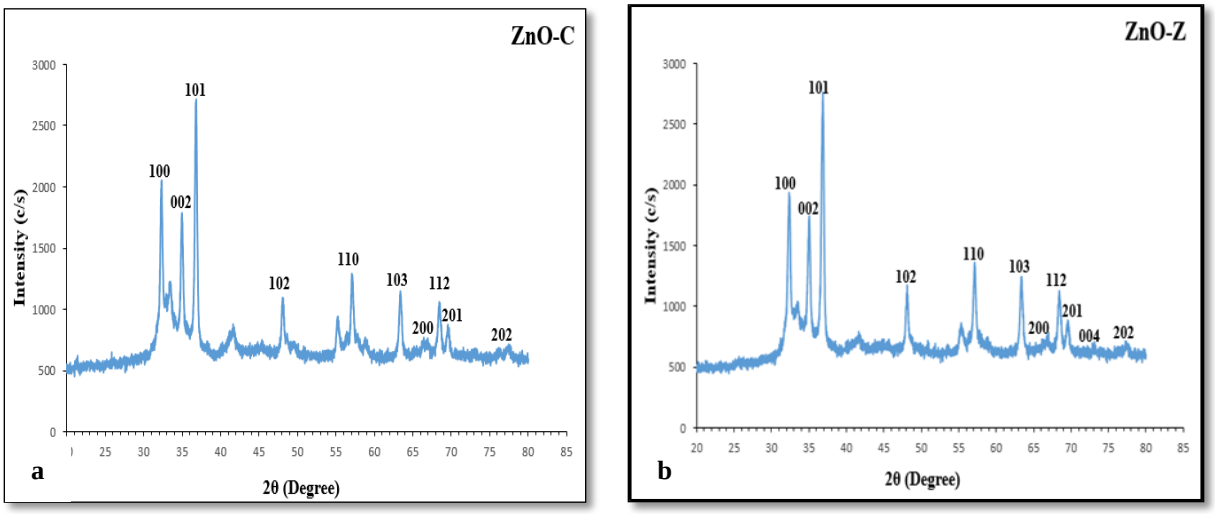


**Figure 4.** XRD pattern for a. ZnO-C NPs ,b. ZnO-Z NPs.

**Table 1.** The X-ray parameters of ZnO-C NPs.

| 2θ (Deg.) Exp | 2θ (Deg.) Std | FWHM (Deg.) | $d_{exp}$(A°) | C.S(nm) | $d_{hkl}$ (A°) | Phase |
|---|---|---|---|---|---|---|
| 32.2708 | 31.928 | 0.4518 | 2.77177 | 11.8 | 100 | Hexagonal JCPDS card :( 96-230-0114) |
| 34.9349 | 34.625 | 0.4366 | 2.56626 | 12.9 | 002 | |
| 36.7528 | 36.445 | 0.3173 | 2.44339 | 23.5 | 101 | |
| 48.0409 | 47.810 | 0.3346 | 1.89233 | 19.2 | 102 | |
| 57.0539 | 56.898 | 0.3735 | 1.61295 | 17.2 | 110 | |
| 63.313 | 63.243 | 0.3886 | 1.46772 | 26.2 | 103 | |
| 66.313 | 66.744 | 0.9364 | 1.40403 | 11 | 200 | |
| 68.3716 | 68.345 | 0.349 | 1.37094 | 23 | 112 | |
| 69.4944 | 69.478 | 0.3778 | 1.3515 | 26.4 | 201 | |
| 77.2869 | 77.424 | 1.3457 | 1.23352 | 4.2 | 202 | |
| | Average of C.S = 17.54 nm | | | | | |

**Table 2.** The X-ray parameters of ZnO-Z NPs.

| 2θ (Deg.) Exp | 2θ (Deg.) Std | FWHM (Deg.) | $d_{exp}$ (A°) | C.S (nm) | $d_{hkl}$ (A°) | phase |
|---|---|---|---|---|---|---|
| 32.2998 | 31.928 | 0.4494 | 2.76935 | 12.5 | 100 | Hexagonal<br>JCPDS card : (96-230-0114) |
| 34.9527 | 34.625 | 0.4594 | 2.56500 | 12.3 | 002 | |
| 36.7736 | 36.445 | 0.3704 | 2.44206 | 20.1 | 101 | |
| 48.0486 | 47.810 | 0.3432 | 1.89205 | 19.1 | 102 | |
| 57.059 | 56.898 | 0.3727 | 1.61282 | 18 | 110 | |
| 63.3075 | 63.243 | 0.4181 | 1.46784 | 25.2 | 103 | |
| 66.6683 | 66.744 | 0.7863 | 1.40176 | 8.7 | 200 | |
| 68.3688 | 68.345 | 0.4140 | 1.37098 | 21.5 | 112 | |
| 69.4806 | 69.478 | 0.3799 | 1.35174 | 22.7 | 201 | |
| 73.0367 | 73.050 | 0.3783 | 1.29445 | 21.3 | 004 | |
| 77.3203 | 77.424 | 1.6016 | 1.23307 | 3.50 | 202 | |
| | Average of C.S = 16.809 nm | | | | | |

## 3.3. Field Emission Scanning Electron Microscopy (FESEM)

Field emission scanning electron microscopy was employed to examine the surface morphology and microstructural characteristics of the synthesized nanoparticles. This technique provides high-resolution imaging that enables accurate observation of particle size, shape, distribution, and surface texture. FESEM analysis is essential for confirming the successful formation of nanostructures and evaluating any agglomeration or morphological features that may influence their physical properties. The obtained images offer detailed insight into the nanomaterial's structural uniformity and help correlate the morphology with the synthesis conditions used.

**Figures 5a** and **5b** displayed the FESEM images of ZnO nanoparticles utilizing *Cordia myxa* extract ZnO-C and *Ziziphus spina* extract samples ZnO-Z, respectively.

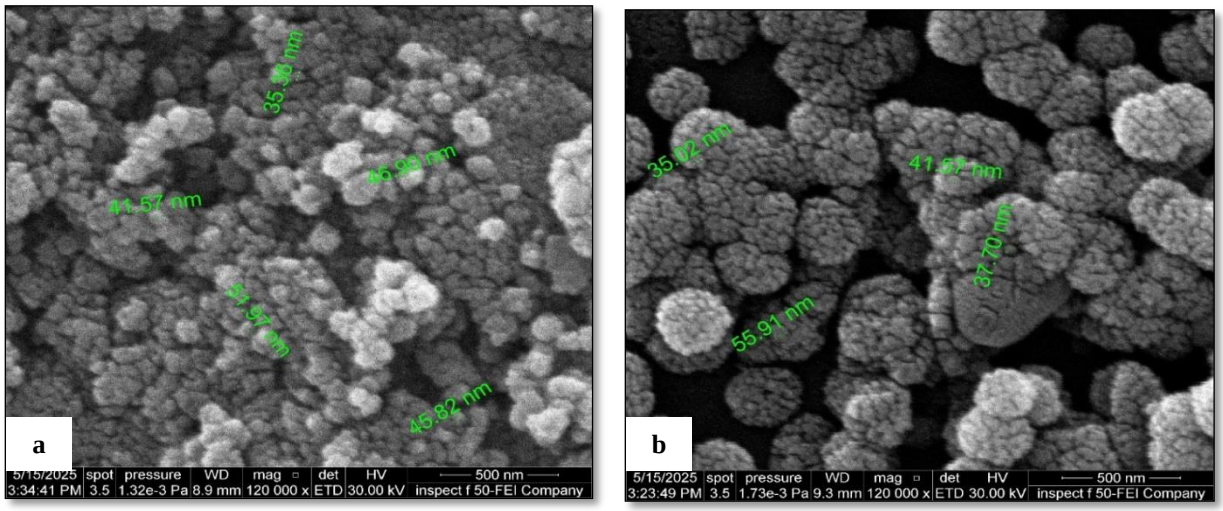


**Figure 5.** Field emission scanning electron microscopy images for **a.** ZnO-C **b.** ZnO-Z

## 3.4. Optical Properties

ZnO nanoparticles prepared from *Cordia myxa* extract and *Ziziphus spina* extract are commonly characterized optically, particularly with UV–Vis spectroscopy to determine their absorption behavior and band gap energy, providing a preliminary assessment of the produced nanoparticles' optical performance. For the ZnO-C sample, the variation of the absorbance spectrum was shown in **Figure 6a**, whereas the variation of $(\alpha h\upsilon)^2$ with $h\upsilon$ was shown in **Figure 6b. Figures 7a** and **7b** illustrated the variation of absorbance with wavelength and the variation of $(\alpha h\upsilon)^2$ with $h\upsilon$ for the ZnO-Z sample, respectively.

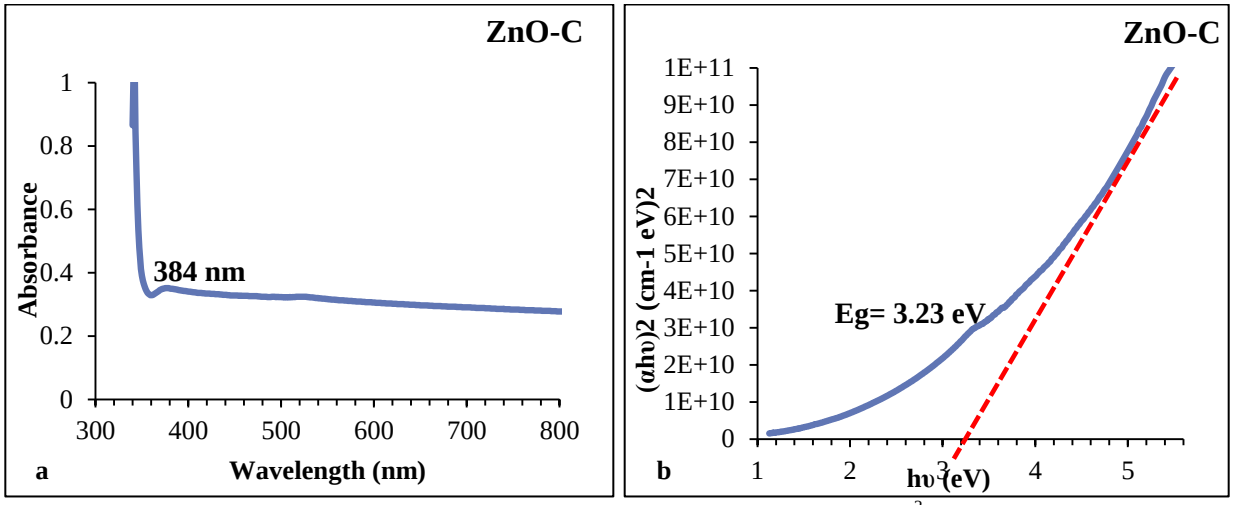


**Figure 6.** a. Absorbance vs. wavelength of ZnO-C, b. Variation of $(\alpha h\upsilon)^2$ vs hυ of ZnO-C

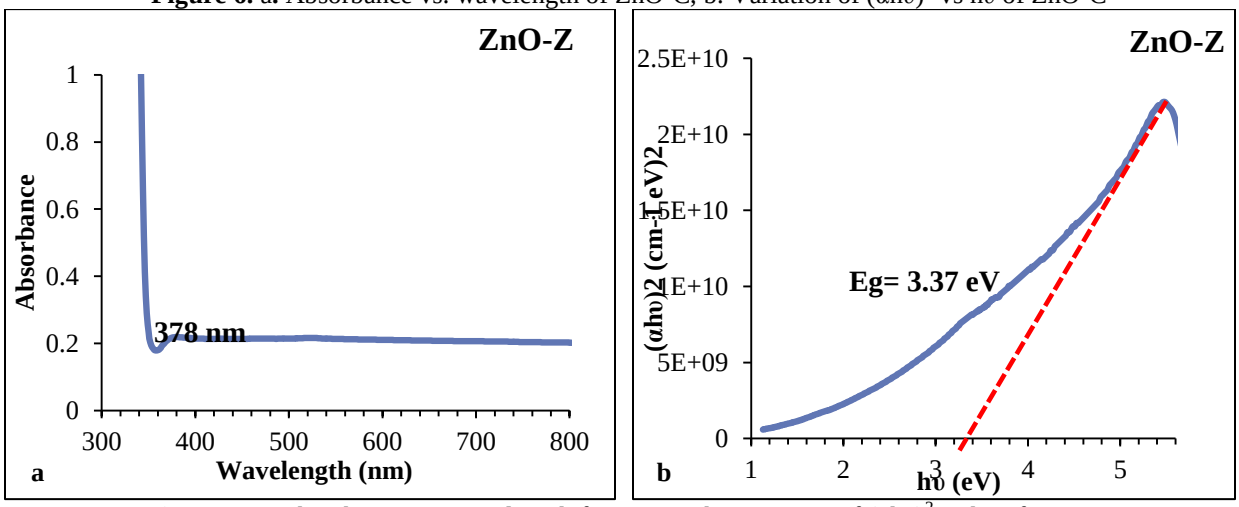


**Figure 7.** a. Absorbance vs. wavelength for ZnO-Z, b. Variation of $(\alpha h\upsilon)^2$ vs hυ of ZnO-Z.

## 4. Discussion

According to **Figures 2** and **3**, the energy dispersive X-ray spectroscopy determines their purity and elemental composition; it is providing information on the percentage of the materials that each element occupies. For ZnO-C, the atomic percentages determined for Zn and O were 64.2% and 35.8%, respectively; it is nearly at the anticipated ZnO stoichiometry, and the weight percentages of Zn are 88.0% and O are 12.0%. The higher weight percentage of Zn is due to Zn being a heavier element compared to oxygen; these values agree with other researchers[26].In the EDX analysis of ZnO-Z elemental composition, the atomic percentages of Zn and O were 71.8% and 28.2%, respectively, and the weight percentages of Zn and O were 91.2% and 8.8%. When compared to ZnO-C, the ZnO-Z sample showed a greater atomic percentage of Zn (71.8%). This rise could be explained by the *Ziziphus spina* extract capping and stabilizing actions, which result in more noticeable ZnO particle nucleation. Reduced oxygen content can also indicate fewer surface-bound oxygen-related flaws. These values were in agreement with that shown for other researchers[27]. The EDX results verify that zinc oxide nanoparticles were successfully formed in both ZnO-C and ZnO-Z samples. The presence of only Zn and O signals without detectable impurities suggests that chemically pure ZnO structures were produced by the biosynthesis process; the slight variations in elemental ratios between the two samples can be attributed to the impact of the plant extracts used during fabrication. For **Figure 4a,** the XRD pattern of ZnO-C prepared samples, the patterns indicated a hexagonal wurtzite phase. The sharp, intense diffraction peaks are observed at diffraction angles of 2θ = 32.2708°, 34.9349°, 36.7528°, 48.0409°, 57.0539°, 63.313°, 66.313°, 68.3716°, 69.4944°, and 77.2869°,

corresponding to the (100), (002), (101), (102), (110), (103), (200), (112), (201), and (202) planes, respectively. The structural parameters of ZnO-C were displayed in **Table 1**, matching the data on the JCPDS card :( 96-230-0114)[28]. The dominant peak for ZnO-C was for plane (101); to determine the dhkl value, Bragg's law was used, according to **Equation 3**[29]:

$$n\lambda = 2 d_{hkl} \sin\theta \quad \textbf{(3)}$$

However, with the Scherrer formula, average crystallite size was calculated for ZnO-C and ZnO-Z nanoparticles, which came out to be 17.54 nm and 16.809 nm, respectively [29,30], according to **Equation 4**:

$$C.S = k\lambda / \beta \cos\theta \quad \textbf{(4)}$$

Where C.S. means the crystallite size of the crystal, k is the shape parameter (0.9), λ is the X-ray wavelength (0.15406 nm), ß is the width of the XRD peak at half height, and θ is the Bragg diffraction angle[10]. **Figure 4b** displayed the X-ray diffraction (XRD) patterns of zinc oxide that were made using *Ziziphus spina* extract. All of the samples possessed a polycrystalline structure, as indicated by the X-ray diffraction peaks, which included eleven peaks at 2θ = 32.2998°, 34.9527°, 36.7736°, 48.0486°, 57.059°, 63.3075°, 66.6683°, 68.3688°, 69.4806°, 73.0367°, and 77.3203°. These crystals were composed of the hexagonal phase of (ZnO-Z) in accordance with the lattice planes (100), (002), (101), (102), (110), (103), (200), (112), (201), (004), and (202), respectively. The values in the standard card number (96-230-0114) match with these values[28]. The dominant peak for ZnO-Z was for plane (101), and **Table 2** demonstrates the X-ray peak parameters of ZnO-Z.In general, in the green-synthesized ZnO nanoparticles' XRD pattern, a slight shift was observed between the experimental 2θ values and the standard 2θ positions (JCPDS card: 96-230-0114)[28]. Such deviations are commonly reported for ZnO prepared via green synthesis and may be attributed to lattice strain, crystallographic defects (such as oxygen vacancies and zinc interstitials), and the influence of phytochemical compounds from the plant extract used during synthesis. Overall, these small variations confirm the formation of ZnO with good crystallinity and are consistent with the nanostructured nature of the prepared material. The FESEM images of ZnO nanoparticles utilizing *Cordia myxa* extract ZnO-C were observed in **Figure 5a** to be spherical, aggregated, and range between 35 and 52 nm in size; the size distribution appears to be moderately wide. Such an aggregation tendency was frequently seen in ZnO that has been green-synthesized [31,32]. Furthermore, based on XRD analysis, the nanoparticles were hexagonal wurtzite, ZnO's most thermodynamically stable crystal structure. This combination of spherical shape and hexagonal crystal structure was in line with earlier research on the green-synthesized ZnO; research has shown that phytochemicals from plant extracts work as reducing and stabilizing agents[33]. Whereas the FESEM image of ZnO nanoparticles by *Ziziphus spina* extract sample ZnO-Z. The aggregation and partial clustering are attributed to the bioactive phytochemicals in the extracts, which act simultaneously as reducing and capping agents, promoting nucleation of ZnO nanocrystals while also inducing particle-to-particle interactions [31,34], and range between 35 and 55 nm in size. Both samples have a rough, porous surface shape, which is useful for processes like photocatalysis and antibacterial activity that need a lot of surface area, as shown in **Figure 5b**. **Figures 6a** and **7a** displayed ZnO nanoparticles produced with *Cordia myxa* extract and *Ziziphus spina* extract analyzed by UV-Vis spectra, respectively. This is because of the valence band's electronic transition to the conduction band; the ZnO-C NPs obtained a strong 384 nm absorption peak. In ZnO, this is due to its intrinsic band-gap absorption. A sharp UV absorption edge confirms ZnO nanoparticle formation. One can conclude that the material is optically transparent by observing the decrease in absorbance with increasing wavelength toward visible and near-infrared wavelengths. This result goes in line with other researchers[35]. The ZnO-Z sample, which was prepared by *Ziziphus spina* extract absorption peak, was shown at 378 nm. This is in agreement with other researchers[36]. Energy gap ($E_g$) was determined by plotting $(\alpha h\nu)^2$ versus hν as illustrated in **Figures 6b** and **7b,** which represent the optical energy gap of ZnO-C, which was equal to 3.23

eV and 3.37 eV, the energy gap for (ZnO-Z). These results are in agreement with the outcomes of other researchers [37,38].

## 5. Conclusions

Utilizing extracts from *Ziziphus spina* and *Cordia myxa* in an aqueous solution of $ZnCl_2$ as natural reducing and stabilizing agents, ZnO nanoparticles were successfully produced in this study utilizing a green technique. EDX, XRD, FESEM, and UV-VIS were the diagnostic methods used to describe the composition, structure, morphology, and optical characteristics of the generated particles. Their purity, nanoscale size, and polycrystalline hexagonal wurtzite structure were all validated by the characterization. This inexpensive and environmentally acceptable method describes how ZnO nanoparticles can be synthesized by plant-mediated synthesis, ZnO-C, and ZnO-Z that are appropriate for optoelectronics, antibacterial, and environmental applications.

## Acknowledgment

We would like to thank the staff of the thin film Lab, Physics Department, College of Sciences, University of Baghdad for their support.

## Conflict of Interest

The authors declare that they have no conflicts of interest.

## Funding

None.

## References

1. Mashrai A, Khanam H, Aljawfi RN. Biological synthesis of ZnO nanoparticles using C. albicans and studying their catalytic performance in the synthesis of steroidal pyrazolines. Arab J Chem. 2017; 10: 1530-1536. https://doi.org/10.1016/j.arabjc.2013.05.004
2. Naser DK, Abbas AK, Aadim KA. Zeta potential of Ag, Cu, ZnO, CdO and Sn nanoparticles prepared by pulse laser ablation in liquid environment. Iraqi J Sci. 2020; 61(10): 2570-2581. https://doi.org/10.24996/ijs.2020.61.10.13
3. Rajabi HR, Naghiha R, Kheirizadeh M, Sadatfaraji H, Mirzaei A, Alvand ZM. Microwave assisted extraction as an efficient approach for biosynthesis of zinc oxide nanoparticles: synthesis, characterization, and biological properties. Mater Sci Eng C. 2017; 78:1109-1118. https://doi.org/10.1016/j.msec.2017.03.090
4. Ramanujam K, Sundrarajan M. Antibacterial effects of biosynthesized MgO nanoparticles using ethanolic fruit extract of Emblica officinalis. J Photochem Photobiol B. 2014; 141: 296-300. https://doi.org/10.1016/j.jphotobiol.2014.09.011
5. Rajeshkumar S, Naik P. Synthesis and biomedical applications of cerium oxide nanoparticles–a review. Biotechnol Rep. 2018; 17: 1-5. https://doi.org/10.1016/j.btre.2017.11.008
6. Dobrucka R. Synthesis of titanium dioxide nanoparticles using Echinacea purpurea herba. Iran J Pharm Res. 2017; 16(2): 756-762.
7. Batool M, Khurshid S, Qureshi Z, Daoush WM. Adsorption, antimicrobial and wound healing activities of biosynthesised zinc oxide nanoparticles. Chem Pap. 2020; 75(3):893-907. https://doi:10.1007/s11696-020-01343-7
8. Sarkar S, Ponce NT, Banerjee A, Bandopadhyay R, Rajendran S, Lichtfouse E. Green polymeric nanomaterials for the photocatalytic degradation of dyes: a review. Environ Chem Lett. 2020; 18(5): 1569-1580. https://doi:10.1007/s10311-020-01021-w
9. Selmi M, Chaabouni F, Abaab M, Rezig B. Studies on the properties of sputter-deposited Al-doped ZnO films. Superlattices Microstruct. 2008; 44(3):268-275. https://doi.org/10.1016/j.spmi.2008.06.005

10. Rasheed RA, Alias MFA. The role of aluminum doping on structural and optical properties of ZnO thin films prepared by PLD. IOP Conference Series: Mater Sci Eng. 2020; 757(1): 012056. https://doi.org/10.1088/1757-899X/757/1/012056
11. Zhaoyang W, Liyuan S, Lizhong H. Effect of laser repetition frequency on the structural and optical properties of ZnO thin films by PLD. Vacuum. 2010; 85(3): 397-399. https://doi.org/10.1016/j.vacuum.2010.07.015
12. Silva RF, Zaniquelli ME. Aluminium-doped zinc oxide films prepared by an inorganic sol–gel route. Thin Solid Films. 2004; 449(1-2): 86-93. https://doi.org/10.1016/S0040-6090(03)01405-6
13. Muslim AM, Naji IS. Antibacterial Activity of Prepared Zinc Oxide Nanoparticles by Eco-Friendly Method Using Olive Leaves and Roselle Flower Extracts. Int J Nanosci. 2024; 23(6): 2450011. https://doi.org/10.1142/S0219581X2450011X
14. Jiang JPiJ, Cai J . The advancing of zinc oxide nanoparticles for biomedical applications. Bioinorg Chem Appl. 2018; 1: 1062562. https://doi.org/10.1155/2018/1062562
15. Madhumitha G, Elango G, Roopan SM. Biotechnological aspects of ZnO nanoparticles: overview on synthesis and its applications. Appl Microbiol Biotechnol. 2016; 100(2): 571-581. https://doi.org/10.1007/s00253-015-7108-x
16. Ali M, Ikram M, Ijaz M, Ul-Hamid A, Avais M, Anjum AA. Green synthesis and evaluation of n-type ZnO nanoparticles doped with plant extract for use as alternative antibacterial. Appl Nanosci. 2020; 10(10): 3787-3803. https://doi.org/10.1007/s13204 020-01451-6
17. Busch G, Schade H, Birman JL. Lectures on solid state physics. Pergamon Press. 1st ed. 1976: 538.
18. Umamaheswari A, Prabu SL, John SA. Puratchikody A. Green synthesis of zinc oxide nanoparticles using leaf extracts of Raphanus sativus var. Longipinnatus and evaluation of their anticancer property in A549 cell lines. Biotechno Rep. 2021; 29: e00595. https://doi.org/10.1016/j.btre. 2021.e00595
19. Elavarasan N, Kokila K, Inbasekar G, Sujatha V. Evaluation of photocatalytic activity, antibacterial and cytotoxic effects of green synthesized ZnO nanoparticles by Sechium edule leaf extract. Res Chem Intermed. 2017; 43(5): 3361-3376. https://doi.org/10.1007/s11164-016-2830-2
20. Aminuzzaman M, Ying LP, Goh WS, Watanabe A. Green synthesis of zinc oxide nanoparticles using aqueous extract of Garcinia mangostana fruit pericarp and their photocatalytic activity. Bull Mater Sci. 2018; 41(2): 1-10. https://doi.org/10.1007/s12034-018 1568-4
21. Greenland K. Measurement and control of the thickness of thin films. Vacuum. 1952; 2(3): 216-230. https://doi.org/10.1016/0042-207X(52)90359-X
22. Gupta V. Mechanical techniques for the measurements of film thickness. Ch 11; Thin Film Science and Technology. 2026.
23. Nagaraja K, Hwan OT. Green synthesis of multifunctional zinc oxide nanoparticles from cordia myxa gum; and their catalytic reduction of nitrophenol, anticancer and antimicrobial activity. Int J Bio. Macromol. 2023; 253: 126788. https://doi.org/10.1016/j.ijbiomac.2023.126788
24. Alharthi MN, Ismail I, Bellucci S, Salam, M A. Green synthesis of zinc oxide nanoparticles by Ziziphus jujuba leaves extract: Environmental application, kinetic and thermodynamic studies. J Phys Chem of Solids. 2021; 158: 110237. https://doi.org/10.1016/j.jpcs.2021.110237
25. Molla A, Hoque M M, Richi FT, Kabir MH, Alam S, Ahmed N U, Emon NU, Shao C, Zeng C, Wang S, Geng P, Mamun, A. A. Biosynthesis and characterization of ZnO nanoparticles using citrus reticulata peel followed by photocatalytic, antibacterial, and antioxidative nanotherapeutic attributes assessment supported by computer simulation. Int J Nanomedicine. 2025; 20: 4803. https://doi.org/10.2147/IJN.S493905
26. Hameed H, Waheed A, Sharif MS, Saleem M, Afreen A, Tariq M, Kamal A, A.Al-onazi W, A.Al Farraj D, Ahmed S, Mahmoud RM . Green synthesis of zinc oxide (ZnO) nanoparticles from green algae and their assessment in various biological applications. Micromach. 2023; 14(5): 928. https://doi.org/10.3390/mi14050928
27. Barzinjy AA, Azeez HH. Green synthesis and characterization of zinc oxide nanoparticles using Eucalyptus globulus Labill. leaf extract and zinc nitrate hexahydrate salt. SN Appl Sci. 2020; 2(5): 991. https://doi.org/10.1007/s42452-020-2813-1
28. Sowa H, Ahsbahs H. High-pressure X-ray investigation of zincite ZnO single crystals using diamond anvils with an improved shape. J Appl Crystallogr. 2006; 39(2): 169-175. https://doi.org/10.1107/S0021889805042457

29. Al-Saadi TM. Investigating the structural and magnetic properties of nickel oxide nanoparticles prepared by precipitation method. Ibn Al-Haitham J Pure Appl Sci. 2022; 35(4): 94-103. https://doi.org/10.30526/35.4.2872
30. Janaki AC, Sailatha E, Gunasekaran S. Synthesis, characteristics and antimicrobial activity of ZnO nanoparticles. Spectrochim Acta A Mol Biomol Spectrosc. 2015; 144: 17-22. https://doi.org/10.1016/j.saa.2015.02.041
31. Abdelbaky AS, Abd El-Mageed TA, Babalghith AO, Selim S, Mohamed AM. Green synthesis and characterization of ZnO nanoparticles using Pelargonium odoratissimum (L.) aqueous leaf extract and their antioxidant, antibacterial and anti-inflammatory activities. Antioxid. 2022; 11(8): 1444. https://doi.org/10.3390/antiox11081444
32. Nhu VTT, Dat ND, Tam LM, Phuong NH. Green synthesis of zinc oxide nanoparticles toward highly efficient photocatalysis and antibacterial application. Beilstein J Nanotechnol. 2022; 13(1): 1108-1119. https://doi.org/10.3762/bjnano.13.94
33. Alharthi MN, Ismail I, Bellucci S, Jaremko M, Abo-Aba SE, Abdel Salam M. Biosynthesized zinc oxide nanoparticles using Ziziphus jujube plant extract assisted by ultrasonic irradiation and their biological applications. Separations. 2023; 10(2): 78. https://doi.org/10.3390/separations10020078
34. Karam ST, Abdulrahman AF. Green synthesis and characterization of ZnO nanoparticles by using thyme plant leaf extract. Photonics. 2022; 9(8): 594. https://doi.org/10.3390/photonics9080594
35. Fouladi-Fard R, Aali R, Mohammadi-Aghdam S, Mortazavi-derazkola S. The surface modification of spherical ZnO with Ag nanoparticles: A novel agent, biogenic synthesis, catalytic and antibacterial activities. J Chem. 2022; 15(3): 103658. https://doi.org/10.1016/j.arabjc.2021.103658
36. MuthuKathija M, Badhush MSM, Rama V. Green synthesis of zinc oxide nanoparticles using Pisonia Alba leaf extract and its antibacterial activity. Appl Surf Sci. Adv.2023; 15:100400. https://doi.org/10.1016/j.apsadv.2023.100400
37. Shoman NA, Salama A, Abbas FG, Mourad HH, Abbas HA. LC-MS/MS profiling and immunomodulatory potential of green-synthesized zinc oxide nanoparticles using Cordia sebestena leaves against chromium-induced acute lung injury in rats. J Drug Deliv Sci Technol. 2025; 106: 106750. https://doi.org/10.1016/j.jddst.2025.106750
38. Saif S, Tahir A, Asim T, Chen Y, Khan M, Adil SF. Green synthesis of ZnO hierarchical microstructures by Cordia myxa and their antibacterial activity. Saudi J Biol Sci. 2019; 26(7): 1364-1371. https://doi.org/10.1016/j.sjbs.2019.01.004